J Mater Sci (2022) 57:20780–20793

Metals & corrosion

Effect of sol–gel treatment on physical, chemical and mechanical stability of copper-coated conductive fabrics: focus on EMI shielding effectiveness

Aravin Prince Periyasamy[1,2,*], Mohanapriya Venkataraman[2], and Jiri Militky[2]

[1] Department of Bioproducts and Biosystems, School of Chemical Engineering, Aalto University, Espoo, Finland
[2] Department of Material Engineering, Faculty of Textile Engineering, Technical University of Liberec, Studentska 2, 46117 Liberec, Czech Republic

Received: 23 July 2022
Accepted: 27 October 2022
Published online: 7 November 2022

ABSTRACT

The development of electronic and communication technology keeps us updated, but it also creates electromagnetic interference (EMI), which causes infrastructure, hospitals, military facilities, nuclear power plants and delicate devices to malfunction. Therefore, it is crucial to stop the EMI-related infrastructure and electronic component failure. Copper-coated textiles are one potential example of the electrically conducting materials that might be utilized to provide an EMI shielding. However, the copper-coated materials' performance is typically reduced by chemical and mechanical deterioration, especially when it comes to EMI shielding. In this work, we have improved their durability of Cu-coated nonwoven fibrous materials (Milife fabric) by simple silanization treatment. Later, the mechanical and chemical stability was assessed in terms of their morphology and EMI shielding effectiveness (EMSE). The silane coating helps to protect the Cu layer from degradation due to mechanical forces and chemical environment. Silanes also be a key element in obtaining improve the EMI shielding properties for a longer period. The formation of conductive structures on the fibrous materials was observed using a scanning electron microscope (SEM), which further confirms the effect of silane coating on chemical stability, abrasion and washing resistance of Cu-coated fibrous materials (cMi) was analyzed. In addition to this, the EMSE values of the silane-coated cMi fibrous materials were used to evaluate the physical, chemical and mechanical stability of the materials.

Handling Editor: Kevin Jones.

Address correspondence to E-mail: aravinprincep@gmail.com

https://doi.org/10.1007/s10853-022-07896-0

Introduction

Research and development of conductive textiles have gained increasing attention in recent years since the science and communication technology have advanced as well as people's pursuit of a healthy lifestyle. Conductive textiles have the lightness and flexibility, and required mechanical properties are suitable to replace the conventional metallic materials [1, 2]. In general, the conductive textiles can be used in different domain including sensors [3], energy harvesting [4], thermal management (i.e., joule heating) [5], antimicrobial [6, 7] and EMI shielding [8, 9].

Recently, electronic devices and communication instruments including the widespread usage of devices that are equipped with fifth-generation (5G) technology are the root cause of EMI [10], which is a dangerous and steadily growing the environmental pollution. The conventional EMI shielding materials were developed using the metal fibers or wires. Generally, the conventional conductive fibrous material requires an additional volume of metal wire or fiber to reach sufficient EMI shielding effectiveness (SE), resulting in consequential increase in weight and non-flexibility [11]. In certain cases, these conductive textiles are rather heavy and do provide a comfortable experience for the wearer.

In most cases, the efficiency of the EMI shielding is determined by the quantity of metal that has been deposited on the fabric. However, the copper-coated textiles have two drawbacks: First, the metal does not have an affinity on the textile materials, resulting the poor durability of the metals, and second, copper-coated textile materials will oxidize when it is exposed to environment, moisture and salt water; as a result, it will reduce the material's capacity to retain its electrical conductivity, EMI shielding effectiveness and thermal conductivity [12]. The development of copper carbonate ($CuCO_3{\cdot}Cu(OH)_2$) on the copper surface was impacted by the degree of air pollution present and the surrounding environment [13]. All these chemical reactions reduce the copper's ability to conduct electricity and protect against electromagnetic radiation, which significantly reduces the conductive fabric's lifetime and limits its use. Therefore, various approach has been conducted to enhance the durability of the copper-coated fibrous materials [14–17]. Consequently, the silver coating can be done to enhance the electrical conductivity [18]. Nevertheless, it is not considered as a pure copper coating; in addition, the silver coating drives up the costs of the process while simultaneously it diverse the properties of final product. Perhaps the method needs several phases, imposes large expenses and would be exceedingly time-consuming when used in industrial manufacturing operations.

Over this, the primary objective of this research was to develop a way that is simple to implement, is of low cost, and saves both time and effort in the process of stabilizing copper particles on fibrous materials. In this research, a unique attempt is made to increase the durability of copper-coated fibrous materials by using a simple sol–gel coating. Therefore, the copper-coated fibrous materials were subsequently coated with five different silanes to achieve the required stability. Overall, all the silanes enhance significantly the mechanical, physical and chemical properties of copper-coated fibrous materials. Thus, the mechanical, physical and chemical properties copper-coated fibrous materials have been analyzed before and after silanization treatment.

Materials and methods

Materials

The combined machine and cross-direction composite nonwoven fabric (Milife) were purchased from JX Nippon ANCI Corporation (sample pMi). Copper-coated Milife was created by Večerník company according to the procedure described in [19]. It is evident from the microscopical picture that the Milife is made up of two layers, with the surface deposition of cuprous particles (Fig. 1). The microscopical images of copper (cMi) and without copper-coated (pMi) fibrous materials are shown in Fig S1. Additionally, Sigma-Aldrich in Prague, Czech Republic, supplied all used chemicals in laboratory standards. Table 1 provides a summary of the sample's fundamental geometrical properties.

Sol–gel synthesis and coating

Five different types of precursors, including tetramethyl orthosilicate (TMOS), tetraethyl orthosilicate (TEOS), triethoxy(octyl)silane (OTES), (3-aminopropyl)trimethoxysilane (APS) and triethoxy(phenyl)silane (PhTES), were employed for

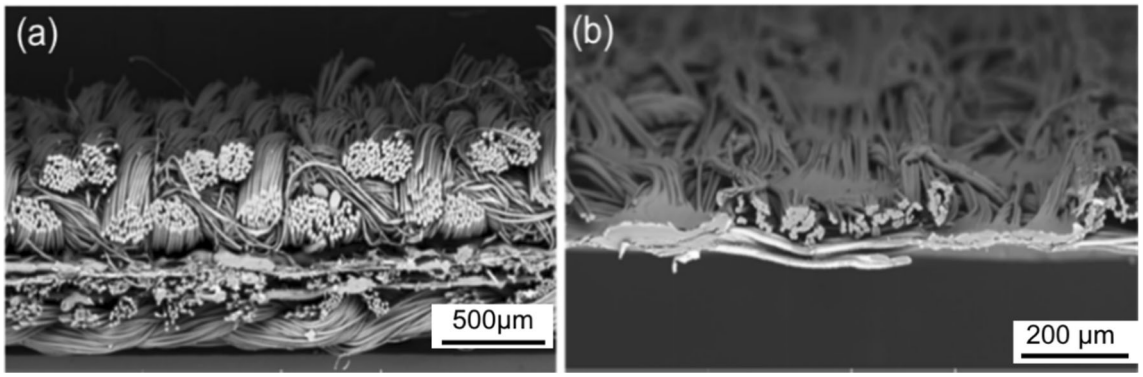

Figure 1 Fabric images of cross-sectional view of pMi (**a**); cMi (**b**).

Table 1 Basic geometrical characteristics of pMi and cMi samples

Type	Areal mass (g.m^{-2})	Thickness (mm)	Density porosity (%)
pMi	11.4 ± 0.252*	0.040 ± 0.026*	79 ± 3.25*
cMi	16.6 ± 1.145*	0.063 ± 0.034*	81 ± 3.68*

*Denotes standard deviation

sol–gel coating. The sols were prepared by mixing the precursors with the catalyst and solvent, and the preparation method was deeply explained in our previous publication [20, 21]. The techniques of dip coating were used in order to coat both cMi and pMi with a different precursor. Later it was dried in atmospheric condition and cured at 110 °C for 10 min. Before EMSE measurement, the sol–gel-coated fabric was left in atmospheric conditions for 24–48 h to ensure complete stabilizing of the silica networks [22].

Testing of coated fabric

Scanning electron microscopy, energy-dispersive X-ray analysis and FTIR

The surface morphology of control and sol–gel-coated fibrous material was observed using a TS5130 Vega-Tescan scanning electron microscope. An energy-dispersive X-ray (EDX) detector (Oxford Inca 200; Oxford Instruments) was utilized and it is connected with a scanning electron microscope to study the chemical composition of conductive fibrous materials. Images were captured at a working distance of 2.5 mm using an acceleration voltage of 20 kV. Attenuated total reflection Fourier transform infrared (ATR-FTIR) spectra of both cMi and pMi before and after sol–gel coating were recorded by a Nicolet Spectrometer (iS10) with *ZnSe ATR crystal*. This spectroscope has coverage of 4000–500 cm^{-1} - spectral region.

X-ray diffraction

In this work, the X-ray diffractometer (from Shimadzu) with Cu Kα radiation generated at a voltage of 40 kV and current of 30 mA is used to record the X-ray diffraction (XRD) patterns of cMi and pMi before and after sol–gel coating. The crystalline structure was studied by evaluating the practices of metal and sol–gel-coated fibrous material using X-ray diffraction using the joint committee on powder diffraction standards (JCPDS) card No. 00-050-2275.

Measurement of EMSE

The electromagnetic shielding efficacy (EMSE) of both cMi and pMi has been evaluated using an EMSE tester over the frequency range of 30 MHz to 1.5 GHz; the testing procedure was followed as per the ASTM D4935-10 [23]. The EMSE measurement testing concepts are described in Fig. 2. During the EMSE measurement, the standard room temperature (21 °C) and relative humidity (55%) were maintained. The EMSE was calculated using Eq. (1), where S_{21} is the forward transmission coefficient and represents the ratio of power without and with shielding

material [24]. Five measurements of each sample were taken at various locations, and the average has been used for further calculations.

$$SE(S21) = -10\log\left(\frac{P_1}{P_2}\right) = 10\log\left(\frac{P_2}{P_1}\right) \quad (1)$$

where P_2 and P_1 are, respectively, the powers received with and without the presence of the fabric. The ratio of the received power with the fabric present P_1 to the received power with the reflection present P_3 is used to compute the input reflection coefficient by using Eq. (2).

$$S_{11} = 10\log\left(\frac{P_3}{P_1}\right) \quad (2)$$

Mechanical stability

The sol–gel-coated conductive fabric was abraded for 10, 20, 30, 40 and 50 cycles under the pressure of 9 kPa in the Martindale abrasion tester concerning the ISO 12947–1:1998 standard. The efficiency of durability can be calculated by the ratio of EMSE values between before and after abrasion measurement. On the other hand, the sample measured their durability against domestic washing according to the AATCC 61-1A method without using steel balls at 40 °C for 45 min using Testex launder-o-meter. All the samples were rinsed twice with water and dried. The EMSE test was conducted both before and after washing to determine their impact.

Chemical stability

The immersion test has been used to evaluate the pMi and cMi fabric's chemical stability both before and after sol–gel. Therefore, the samples were immersed for 72 h in water, boiled water, 1 M NaCl, 1 M NaOH, 1 M HCl, 1 M CH_3COOH and organic solvent like ethanol. After 72 h, the conductive fibrous materials have been analyzed to understand the loss of EMSE.

Physical properties

According to ASTM D1777, the thickness of the pMi and cMi fibrous material was tested using a thickness gauge tester, and areal density was computed based on the ASTM D3776-07 standard. In Textest FX 3300, according to ISO 9237, the air permeability of the pMi and cMi samples was measured. The mass add-on percentage of the silanized cMi fabric was computed with the help of the following equation.

$$M = \left(\frac{S_1 - S_0}{S_0}\right) \times 100\% \quad (3)$$

where M is mass add-on percentage and S_0 and S_1 are the mass of substrate before and after sol–gel coating, respectively.

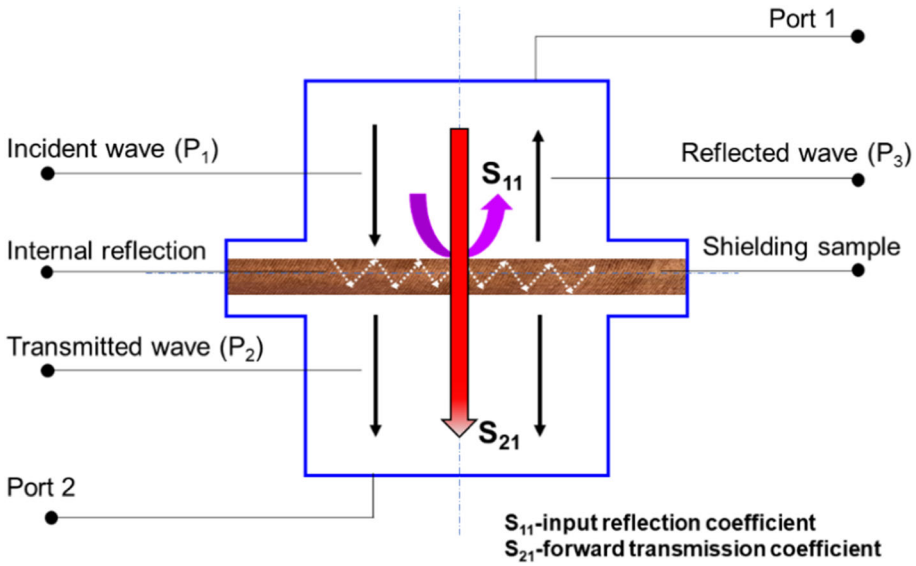

Figure 2 Measurement of EMSE for Cu-coated polyester fibrous materials.

Results and discussion

Surface morphology of pMi & cMi fabric

The morphological properties of conductive Milife (cMi) and pristine Milife (pMi) fibrous material were examined using SEM, and the micrographs are shown in Fig. 3. Figure 3a and Fig. 3b illustrates the cross sections of pMi and cMi, respectively. Figure 3c, d shows the surface profile of with and without copper coating on the Milife fabric as it provides an idea of the surface layers of copper (i.e., cuprous layer). As a result, sol–gel coating proved that the copper coating on the fabric is stabilized completely and uniformly covers the fiber surface, as is seen in the SEM images (Fig. 3e and f). Si sols were dispersed evenly on the cMi samples that are shown in Fig. 3f. On the contrary, Fig. 3e shows the uneven coating of copper on the fabric surface without sol–gel coating. Hence, Si–O–Si sols form a thin film layer on the cMi fabric surface that is more uniformly distributed, but the film thickness is dependent on the type of silane and viscosity [25–27]. The loss of electromagnetic waves due to multiple reflections and scattering increases with the deposition of Cu on fibrous materials. Additionally, the Cu particles that are deposited after silanes form a thin coating have a large specific surface area, which is crucial and improves EMI shielding efficiency.

In our previous study [20], we investigated the effect of sol–gel treatment on the surface roughness of copper-coated nonwoven materials by using of confocal microscope and the results were compared to those obtained without the treatment. The properties of the roughness vary greatly depending on the type of silane that was utilized. Thus, PhTES has the lowest surface roughness characteristics as it is containing cyclic ring and hence provides the rigid three-dimensional silica network on the copper-coated fibrous materials. On the other hand, the silane containing long aliphatic groups (i.e., OTES) provides the higher surface roughness and the resultant fibrous material provides soft and more flexibility. Additionally, EDS mapping and analysis were done to determine the distribution and elemental detection of copper particles on the polyester fibrous material. Figure 4 shows the homogeneous distribution of the elements Cu, Ni, Ti, C and O. The presence of copper

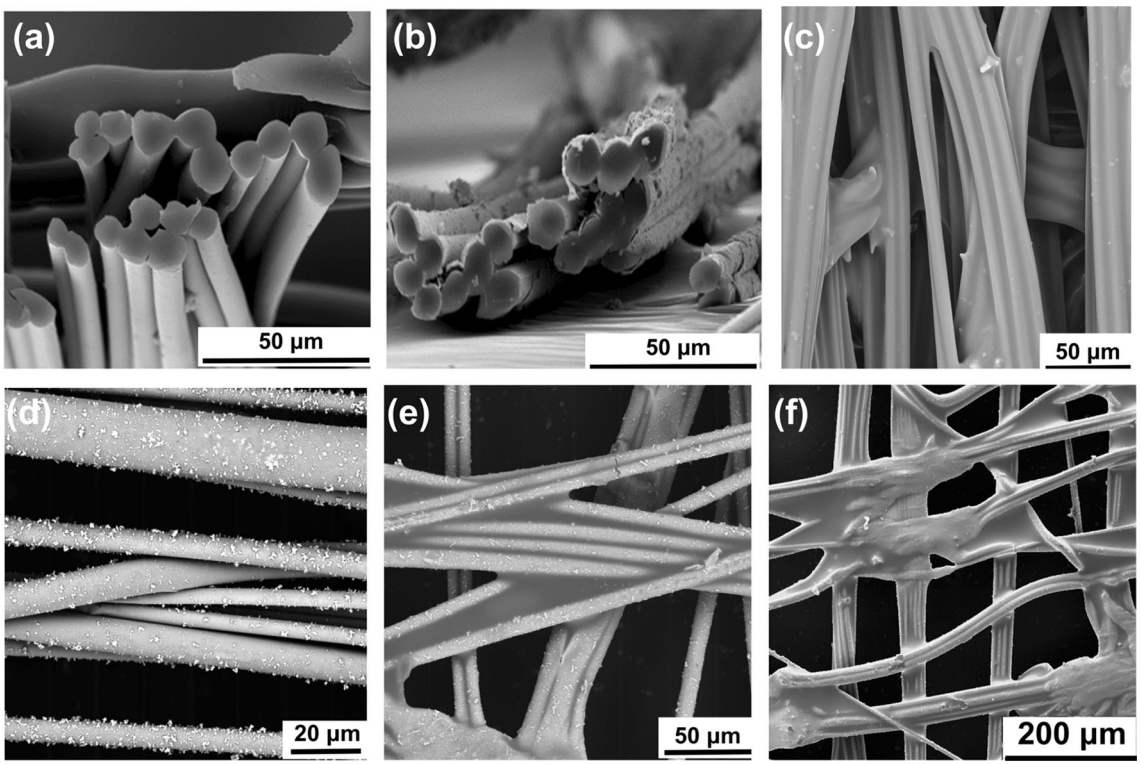

Figure 3 Cross section of pMi (**a**), cMi (**b**); surface view of pMi (**c**) cMi (**d**) and the influence of sol–gel treatment on the cMi (**e**) OTES; (**f**) PhTES.

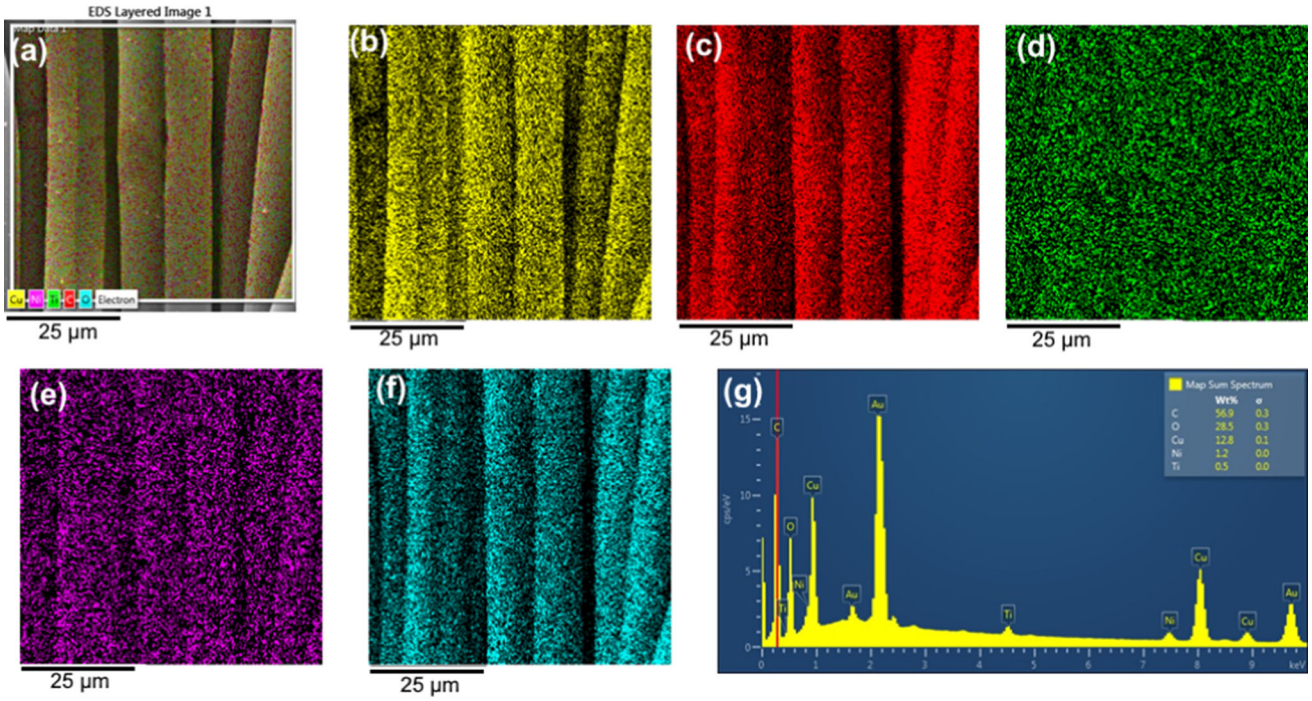

Figure 4 EDS mapping (**a**–**f**) and spectra (**g**) of the cMi fibrous material.

on the surface of polyester fiber materials has been confirmed by EDX analysis (Cu wt% is 12.8, Ni wt% is 1.2%). The weight percentage of each element in the cMi fabric is shown in Fig. 4g.

FTIR characterization on fibrous materials

The impact of silane treatment, as well as copper deposition on the fibrous material, is analyzed using ATR-FTIR spectroscopy, and the results are presented in Fig. 5. The peak 1017 cm^{-1}, 1711.53 cm^{-1}, 1096 cm^{-1} and 1242 cm^{-1} (C=O) connects to ester groups confirm the deformation of CH_2 and CH_3 groups. Also, the peak identified between 1300 and 1000 cm^{-1} resembles the C=O stretch in ester groups of polyester materials. The strong characteristic peaks at 780 cm^{-1} and 820 cm^{-1}, respectively, establish the (Si–CH) bonds in silane-treated cMi fibrous material. The intensity peaks between 1090 and 1190 cm^{-1} are due to increased Si–O–C, Si–O–Si and Si–C bonds on sol–gel-coated fabric [28, 29]. The methoxy groups of TMOS confirm the peaks at 1090 cm^{-1} (Si–O–CH_3). The intensity of all inherent peaks has decreased as a result of Cu deposition on the fibrous material, as shown in Fig. 5. Short peaks in the ranges of 1713 cm^{-1} to 1627 cm^{-1} and 1555 cm^{-1} to 1425 cm^{-1} have been identified, indicating that the fibrous material is heavily integrated with Cu [20, 30]. Furthermore, the sulfate group has been established in the range of 1415 cm^{-1} to 1380 cm^{-1}, and it is typically found in copper-plated fibrous material.

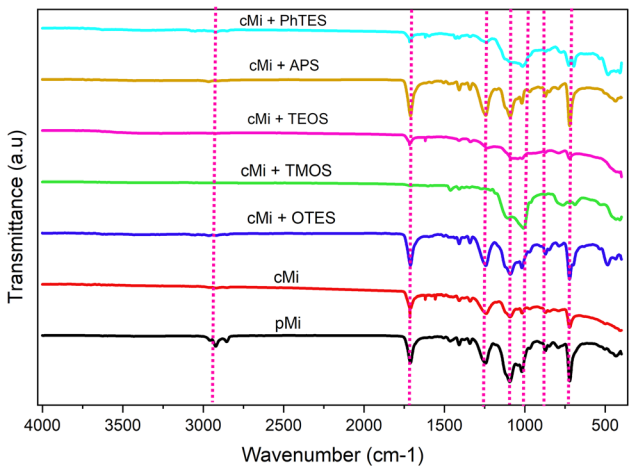

Figure 5 FTIR spectra of pMi, cMi and silane-treated cMi fibrous material.

XRD characterization of pMi & cMi fabric

The XRD patterns of the pMi and cMi fibrous material are shown in Fig. 6. According to the Joint

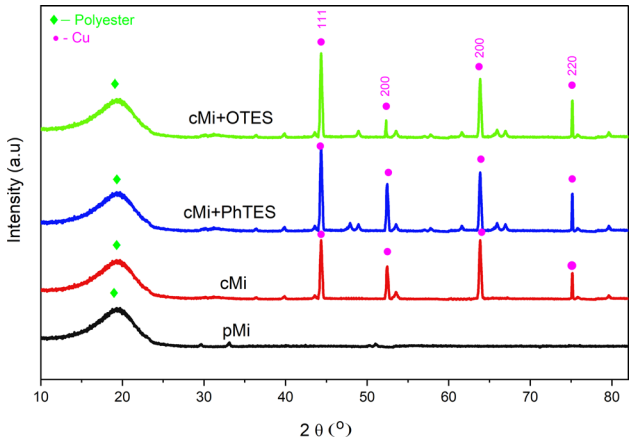

Figure 6 XRD spectra of pMi, cMi and silane-treated cMi fibrous material.

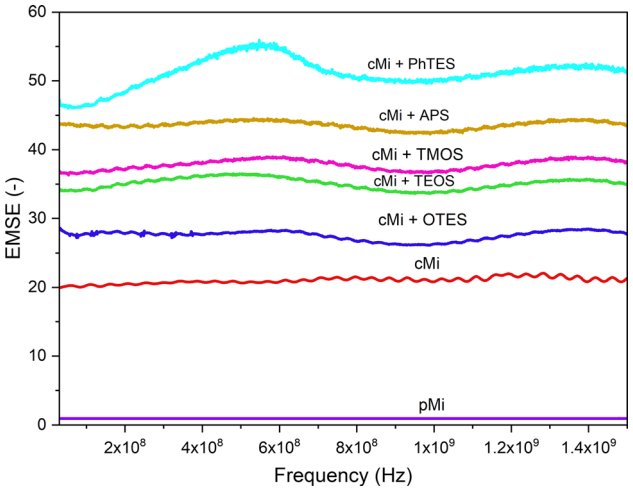

Figure 7 Influence of silane treatment on EMSE values of pMi, cMi fibrous materials.

Committee on Powder Diffraction Standards, JCPDS card number. 00-050-2275, the pMi fabric has large peaks at 20.0°, which correspond to crystal planes of (011) polyester structure [31]. After copper is deposited, cMi fibers have a significant impact on the crystalline structure of PET fibrous materials. This is primarily due to copper deposition on the surface of the fibrous material. Apart from PET fabric peaks, Cu signals can be seen in the diffraction pattern of cMi fibrous materials with $2\theta = 44.3°$, 52.3°, 63.8° and 75.2°, which correspond to the (111), (200), (220) and (311) crystal planes of metallic copper, respectively (JCPDS card number. 85-1326) [32–34]. After sol–gel (i.e., PhTES) coating, the peaks observed at 36.8° and 39.3° were indexed as the (1 1 1) and (2 0 0) of Cu particles with cubic crystallographic structure. On the other hand, the precursor that was used does not have a significant impact on it. The PhTES comprises of phenyl group implemented as a precursor that does not have any evidence of a strong peak. A similar trend was observed for OTES. The characteristic diffraction peaks of polyester credit to the broad diffraction peaks of each sample at 17.1°, 22.4° and 25.4°. The amorphous nature of PET fabrics is reflected around a 20° intense peak.

EMI shielding

The coaxial transmission line method is used to examine the EMSE of cMi, pMi and silane-treated cMi with respect to the ASTM standards [35], and the results are shown in Fig. 7. All the samples were evaluated at frequencies ranging from 30 MHz to 1.5 GHz, with the SE displayed in decibels (dB). Overall, the silane treatment yields promising results and significantly improve the EMSE values. However, it depends on the type of silane used for the sol–gel coating. Due to the failure of attenuation of the electromagnetic field, when the fabric is not coated with copper (pMi), it exposes a certain effectiveness in shielding performance ($\sim$ EMSE > 1). The values are inversely related to frequency (Fig. 7). Perhaps, the findings are known: The presence of copper alone is insufficient to produce the necessary positive electromagnetic shielding effectiveness.

Shielding behavior versus sol–gel treatment

As previously indicated, the silane treatment improves the EMSE values significantly; the cMi-PhTES fabric has the greatest SE value of 46 dB at the lowest frequency (30 MHz) and 52 dB at 1.5 GHz, and the SE increases logarithmically with frequency. The SE of the cMi-PhTES fabric is roughly 52 dB at 1.5 GHz, indicating a "very good" SE (see Table S1) for all tested frequencies.

Comparatively, the shielding effectiveness for cMi with PhTES is approximately double the amount than that pMi fabric (Fig. 7), which shows the promising and novel results from this work. As a consequence of extremely excellent shielding effectiveness, values observed with cMi with APS are very good above 43 dB at 30 MHz and fall to 40 dB when the frequency is increased to 1.5 GHz. The increased EMSE values are due to the chemical structure of PhTES and APS, which has an aromatic ring that absorbs

electromagnetic energy through strong bonding interactions inside the cyclic ring. The carbon–carbon, carbon–hydrogen and benzene ring lay in one torus, improving the cMi-PhTES fabric's shielding efficiency.

Furthermore, the shielding performance of OTES on cMi is consistent from the lowest to the highest frequency. When compared to OTES with cMi, TMOS with cMi exhibits greater electromagnetic shielding efficacy in the case of TEOS. In general, TEOS and OTES included flexible aliphatic alkoxysilane incapable of absorbing electromagnetic radiation, reducing the efficiency of shielding. Textiles can be categorized into five categories, ranging from a fair grade to an outstanding grade, in accordance with the standards for EM shielding textiles, based on their intended professional or general use (see Table S1). While general usage is represented by casual clothing, maternity wear, aprons, shielding of consumable electronic devices and communication-related products, etc., professional use includes professional protective uniforms for electronic producers and shielding of medical equipment.

Durability measurement

Abrasion resistance

The Martindale test measured the abrasion resistance of the cMi and pMi textiles deposited with silane coatings. These findings suggest that the type of silane employed has a significant impact on abrasion resistance (Fig. 8). Since the silane chemistry decides the surface characteristics of the coated fabric, it was assumed that such a hybrid sol (i.e., PhTES, APS) might be used to make xerogel coatings that are brittle and have low abrasion resistance. In the Martindale test, the silane treatment allowed perfect fiber protection against abrasion after 50 cycles of abrasive head motion. At 50 abrasion cycles, the EMSE values at 1.5 GHz for the precursor with OTES were lowered by 17%, despite ES declining by 28% and APS by 24% at the same abrading intensity. The findings of the EMSE values before and after abrasion resistance demonstrate that the precursor types have a nonlinear relationship. The results of the EMSE value % on the abrasion cycles (in all levels) were in the order of PhTES > APS > TEOS > TMOS > OTES.

Figure 9 shows the morphological changes of the fabric after abrasion cycles. It can be observed that

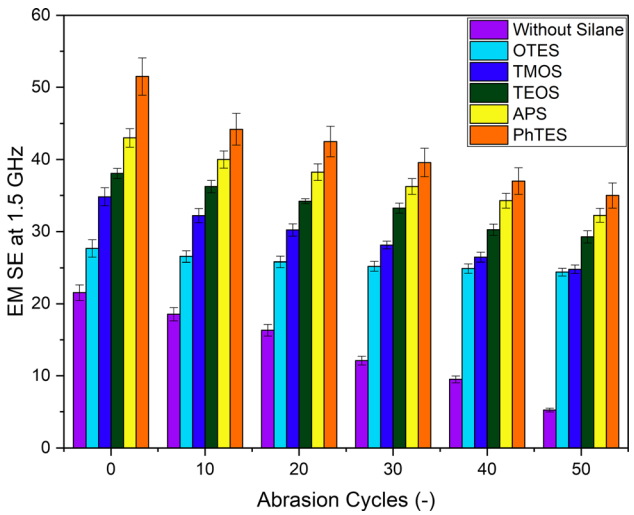

Figure 8 Influence of silane treatment on abrasion resistance of cMi fabric.

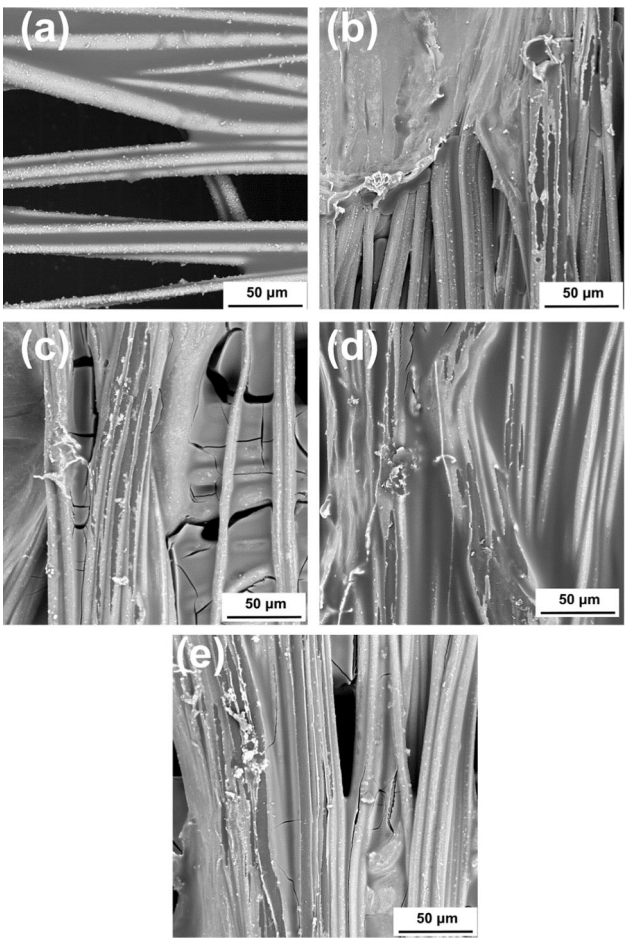

Figure 9 Morphological analysis 50 cycle abraded cMi-PhTES (**a**), cMi-APS (**b**), cMi-TEOS (**c**), cMi-TMOS (**d**), cMi-OTES (**e**).

the deposition of copper on the PhTES-coated fabric stabilized (Fig. 9a) and was not affected as compared to the cMi-OTES fabric (Fig. 9e).

Washing resistance

The washing durability of the cMi fabric before and after sol–gel treatment was evaluated by the AATCC standard washing test. The EMSE test was carried out after different washing cycles. The assessment of washing durability of pMi and cMi along with silane treatment is shown in Fig. 10. Overall, the washing durability of silane-treated pMi and cMi fabric on their EMSE values is varied concerning the type of precursor. After 5 washing cycles, there is a drastic reduction in EMSE for the samples without sol–gel coating (47% loss); meantime, the samples with sol–gel coating show variant to the decrease in EMSE. The cMi-OTES fabric's washing durability has been reduced by 19.5% of EMSE values, which is a very high EMSE loss percent after the silane treatment. On the other hand, the cMi-PhTES fabric has only 3.8% EMSE loss, while APS has a 12% loss, so the overall level of washing durability is satisfactory except for OTES. The chemistry of the silane is directly influenced by this phenomenon since the aliphatic structure is easily hydrolyzed, and the bond breakage leads to the loss of EMSE values. Figure 11 shows the morphological changes of the fabric after washing. It can be observed that the deposition of copper on the PhTES-coated fabric stabilized and was not affected as compared to the cMi-OTES fabric.

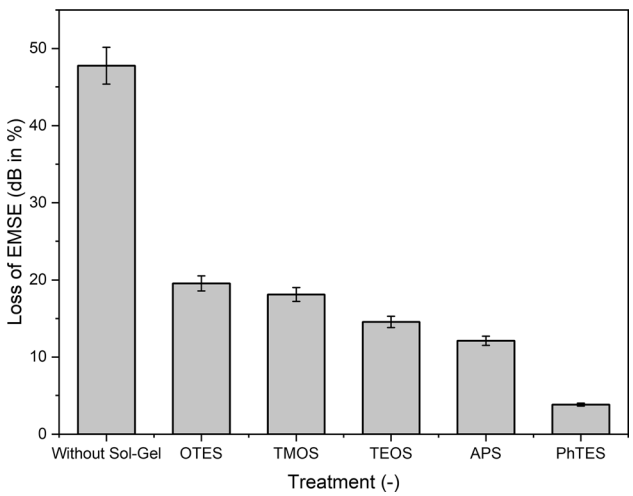

Figure 10 Loss of EMSE% on standard washing conditions.

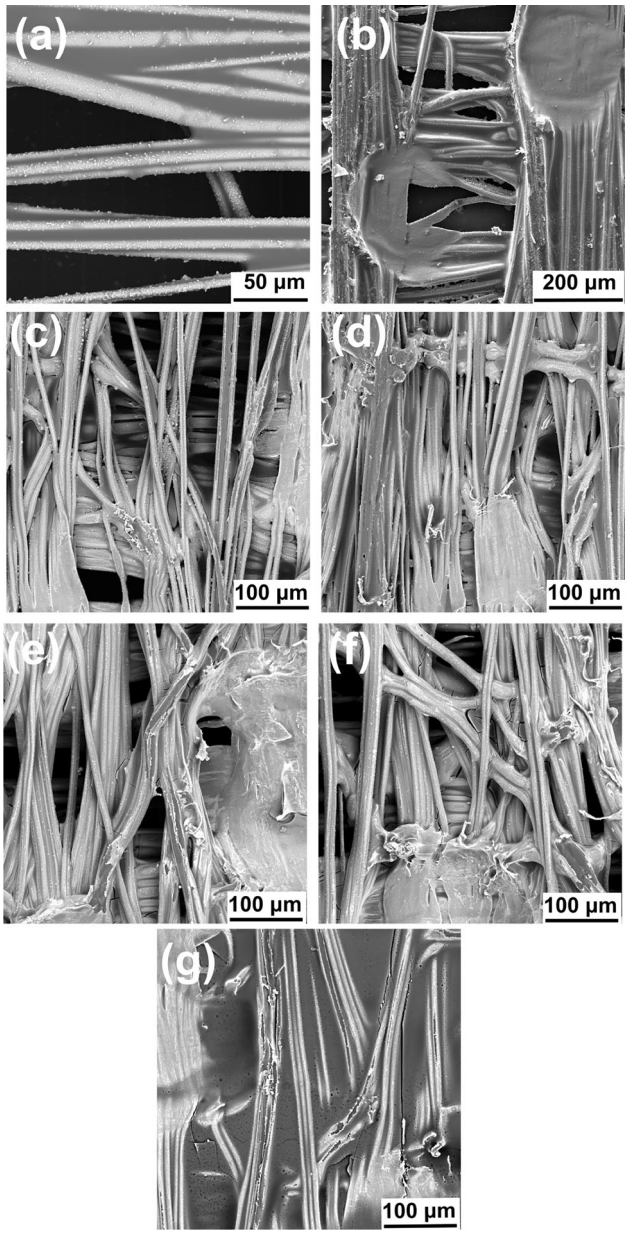

Figure 11 Microscopical changes after washing cMi (**a**), without silane treatment (**b**), OTES-cMi (**c**), TMOS-cMi (**d**), TEOS-cMi (**e**), APS-cMi (**f**) and PhTES-cMi (**g**).

Chemical stability

The chemical stability of cMi fabric before and after the sol–gel coating has been assessed by the immersion test in consideration of the diverse application environment of EMI shielding applications. Conductive fabric's chemical stability was tested during a 72-h submersion in water, boiling water, 1 M NaCl, 1 M NaOH, 1 M HCl, 1 M CH_3COOH and ethanol. The stability of EMSE (dB) can be calculated before

and after the chemical stability experiment. The results are shown in Fig. 12.

Among the chemical stability measurements, 1 M of CH_3COOH strongly influences the reduction of EMSE values, followed by 1 M HCl. In general, copper is not damaged by acidic environments. Hence, copper cannot replace the hydrogen in HCl to create $CuCl_2$, so Cu does not react with HCl because Cu has a larger reduction potential than hydrogen. However, the interaction of copper with acids depends significantly on oxygen. Even in the presence of non-oxidizing acids like HCl, when copper (II) chloride ($CuCl_2$) or copper chloride ($Cu_2(OH)3Cl$) are generated, the oxidative corrosion of the copper surface is quick when oxygen or other oxidizing agents are present. Acetic acid and copper-coated PET fabric have the potential to produce copper (II) acetate [36]. A free radical is created as a result of the interaction of copper, acetic acid and ambient oxygen, resulting in the start of an electrochemical corrosion process. The simple process of creating copper (II) acetate is shown in Eq. (4).

$$Cu + 2CH_3COOH + O_2 \rightarrow Cu(CH_3COO)_2 + H_2O \quad (4)$$

$$CuSO_4 + 2NaOH \rightarrow Cu(OH)_2 + Na_2SO_4 \quad (5)$$

Alkali corrodes copper gradually, but the process is noticeable. However, it continued oxidation in a diluted NaOH solution (Eq. 5), and the activity is more pronounced when the metal is in simultaneous contact with both air and water.

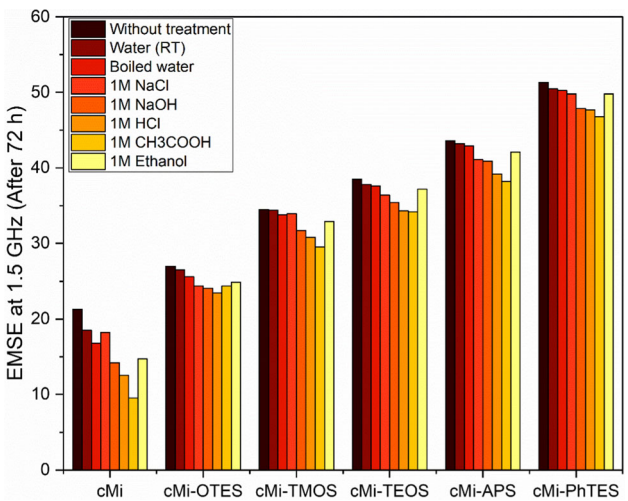

Figure 12 Loss of EMSE at 1.5 GHz with different chemical environments on cMi fibrous materials.

The surface morphology was assessed and is shown in Fig. 13. The silane coating is peeled off in a few spots on the cMi fabric submerged in NaOH, as shown in Fig. 13e, resulting in the drop of EMSE (Fig. 12). The sol–gel (PhTES)-coated cMi fibrous materials show very good durability to the acidic, alkaline and organic solvent condition. Overall, the silane-treated cMi fibrous materials demonstrated acceptable durability concerning the chemical

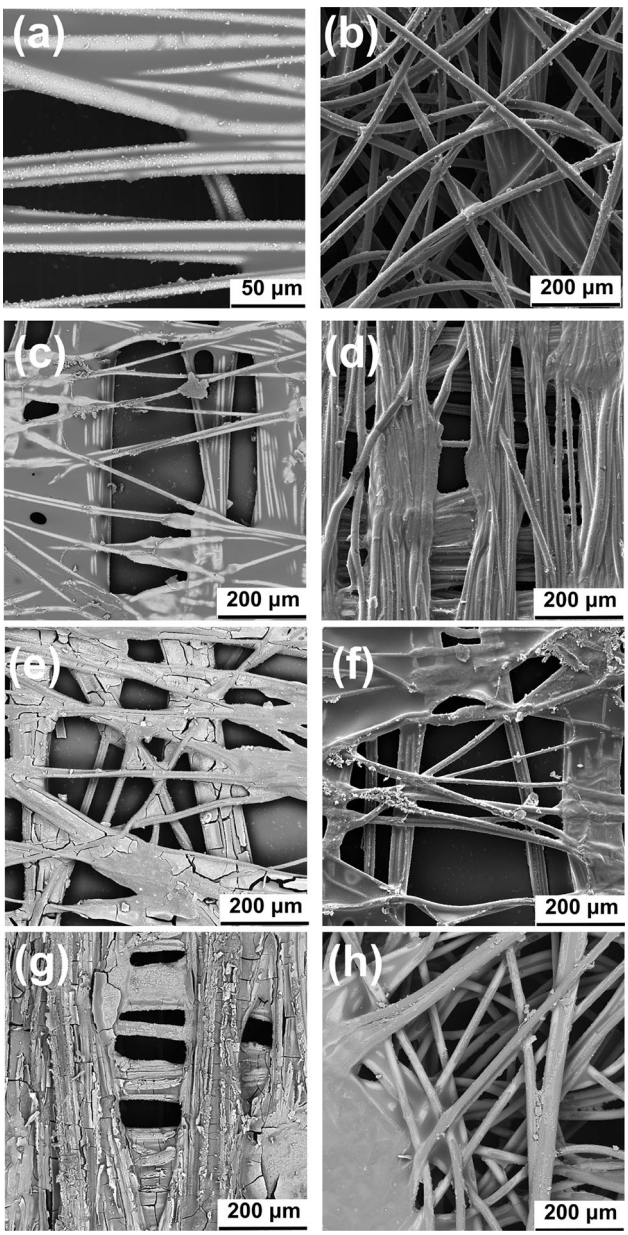

Figure 13 Microscopical analysis of cMi fabric (**a**) 72-h immersion of cMi-PhTES with water (**b**), boiling water (**c**), 1 M NaCl (**d**), 1 M NaOH (**e**), 1 M HCl (**f**), 1 M CH_3COOH (**g**) and ethanol (**h**).

environments to which they are frequently exposed in daily life. Figure 14 shows the possible degradation of silane under a strong acidic and alkaline medium [37–39].

Physical properties

Air permeability

The pMi and cMi fibrous material air permeability was examined, and the findings are displayed in Fig. 15. Overall, the silane treatment results in a decrease in air permeability. As measured by values ranging from 800 to 850 mm/s, there was no discernible difference in the air permeability between cMi with cMi-OTES and cMi-TMOS, while the lowest air permeability was found with cMi-PhTES. The rigid PhTES layer deposition on the fiber's surface might cause the reduction in the air permeability. Comparing the silane-treated cMi fabric to other work [40], the high air permeability (> 600 mm/s) overall supported the breathability of the fabric.

Thickness and areal density of coated fibrous material

The analysis of the fabric's thickness is summarized in Table 2. Results indicate a strong correlation between fabric thickness and coating method. However, a certain precursor has strong effects on the fabric's thickness. The cMi-OTES and cMi fibrous materials would not differ significantly in terms of their thickness. However, the rigid structure of silica

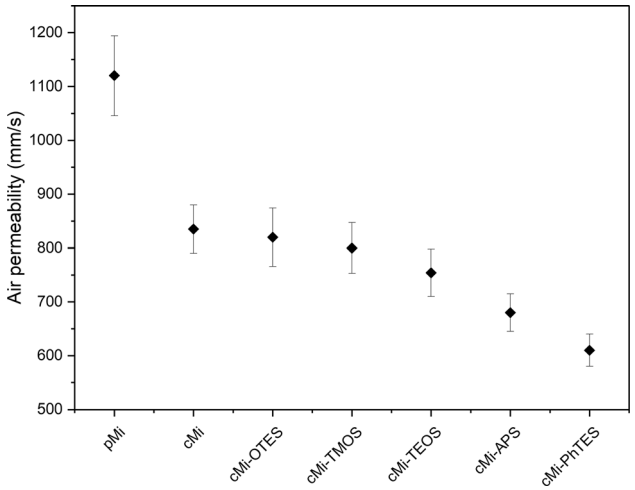

Figure 15 Influence of silanization process on the air permeability of cMi fibrous materials.

networks is often causing the increased fabric thickness on fabric (cMi) treated with APS and PhTES. The areal density of any substrate changes when other materials are deposited on it; in our scenario, the sol–gel-coated samples exhibit a higher areal density than the cMi fibrous materials. The overall results are summarized in Table 2.

Conclusion

This investigation aims to assess the physical, chemical and mechanical stability of Cu-coated fibrous materials (i.e., Milife fabric). In this work, we

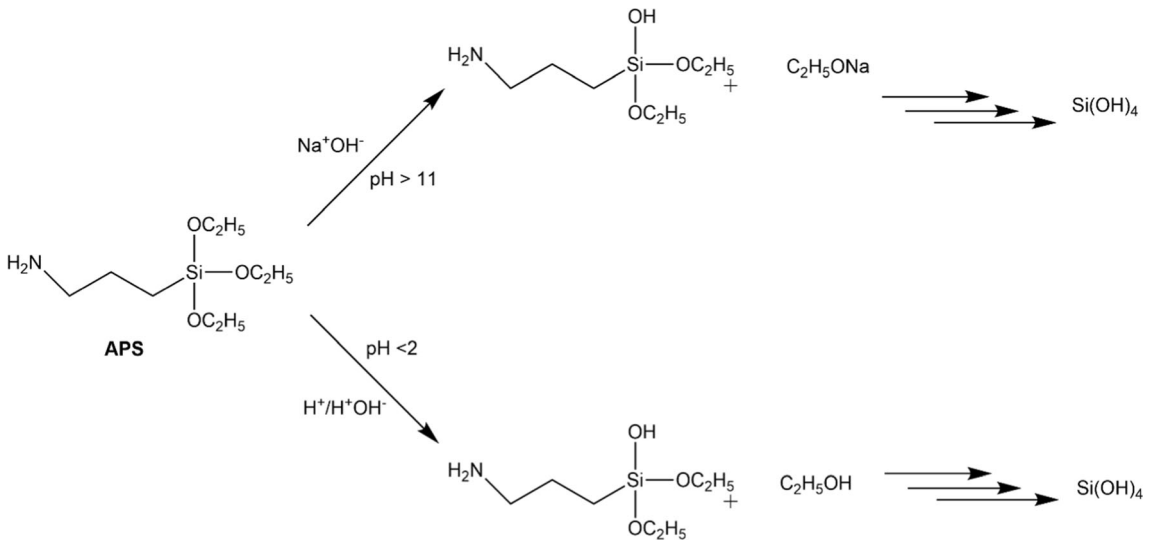

Figure 14 Effect of the acidic and alkaline environment with their chemical degradation on the.

Table 2 Basic geometrical characteristics of pMi and cMi samples

Type	Areal mass (g m^{-2})	Thickness (mm)	Density porosity (%)	Mass add-on %
pMi	11.4 ± 0.252*	0.040 ± 0.026*	79 ± 3.25*	–
cMi	16.6 ± 1.145*	0.063 ± 0.034*	81 ± 3.68*	–
cMi-OTES	16.7 ± 1.025*	0.064 ± 0.009*	82 ± 3.87*	4.4
cMi-TMOS	16.9 ± 0.958*	0.064 ± 0.011*	82 ± 2.95*	4.8
cMi-TEOS	17.1 ± 0.854*	0.064 ± 0.019*	83 ± 3.24*	5.2
cMi-APS	17.2 ± 0.747*	0.065 ± 0.017*	85 ± 3.88*	6.4
cMi-PhTES	17.8 ± 0.724*	0.067 ± 0.025*	88 ± 2.99*	8.4

*Denotes standard deviation

have used simple sol–gel coating on the Cu-coated fibrous materials with different silanes. Sol–gel coating was achieved on the Cu-coated fibrous materials without compromising the core characteristics. In general, the findings show that the use of Cu stabilization on cMi fibrous materials is successful in opening doors for the realization of future applications in smart textiles, particularly on the EMI shielding. Overall, the silane-treated cMi fibrous materials show two times higher EMSE values and the chemistry of the silanes plays a vital role. The ensuing EMSE and the stability of the Cu particles were both improved on the cMi fibrous materials as a result of the sol–gel coating. Both properties are extremely important, and it enhanced in this work. Additionally, the chemical resistance, abrasion and washing resistance of sol–gel-coated cMi fibrous materials has been improved. From the results, it can be concluded that the silane treatments improve the physical, mechanical and chemical stability of cMi fibrous materials. Moreover, to validate the silica networks on the sol–gel-coated fabrics, FTIR studies observed the intense peaks between 1090 and 1190 cm^{-1} confirming Si–O–C, Si–O–Si and Si–C bonds on the sol–gel-coated cMi fabric, XRD analysis differentiates and confirms the Cu deposition on the fibrous materials. In both abrasion and washing resistance experiments, PhTES offers the lowest loss of EMSE values among the various silanes, and its order is PhTES > APS > TEOS > TMOS > OTES. Nonetheless, 72-h immersion of silanized cMi fibrous material in acetic acid significantly affects the EMSE values, since acetic acid and copper-coated PET fabric have the potential to produce copper (II) acetate; however, the results of silanized cMi fibrous material are far better than cMi fabric.

Acknowledgements

The authors would like to thank Arvind Negi., Ph.D, for his comments and the two anonymous reviewers for their insightful suggestions and careful reading of the manuscript.

Funding

Open Access funding provided by Aalto University. This work was supported by the Ministry of Education, Youth and Sports of the Czech Republic and the European Union—European Structural and Investment Funds in the frames of Operational Programme Research, Development and Education—project Hybrid Materials for Hierarchical Structures (HyHi, Reg. No. CZ.02.1.01 /0.0/0.0/16_019/0000843).

Declarations

Conflict of interest The authors declare no conflict of interest.

Supplementary Information: The online version contains supplementary material available at https://doi.org/10.1007/s10853-022-07896-0.

References

[1] Kelvin) Fu K, Padbury R, Toprakci O et al (2018) Conductive textiles. In: Miao M, Xin JH (eds) Engineering of high-performance textiles. Woodhead Publishing, pp 305–334

[2] Yang K, Periyasamy AP, Venkataraman M et al (2020) Resistance against penetration of electromagnetic radiation for ultra-light cu/ni-coated polyester fibrous materials. Polymers (Basel) 12:2029. https://doi.org/10.3390/polym12092029

[3] Lee J, Kwon H, Seo J et al (2015) Conductive fiber-based ultrasensitive textile pressure sensor for wearable electronics. Adv Mater 27:2433–2439. https://doi.org/10.1002/adma.201500009

[4] Lv J, Jeerapan I, Tehrani F et al (2018) Sweat-based wearable energy harvesting-storage hybrid textile devices. Energy Environ Sci. https://doi.org/10.1039/C8EE02792G

[5] Pakdel E, Naebe M, Sun L, Wang X (2019) Advanced functional fibrous materials for enhanced thermoregulating performance. ACS Appl Mater Interfaces 11:13039–13057. https://doi.org/10.1021/acsami.8b19067

[6] Shi H, Kremenakova D, Militký J, Periyasamy AP (2021) Copper-coated textiles for viruses dodging. In: Militký J, Periyasamy AP, Venkataraman M (eds) Textiles and their use in microbial protection: focus on COVID-19 and other viruses. CRC Press, Boca Raton, FL, pp 235–250. https://doi.org/10.1201/9781003140436-14

[7] Hu S, Wang D, Yang K, et al (2020) Copper coated textiles for inhibition of virus spread. In: Textile bioengineering and informatics symposium proceedings 2020 - 13th textile bioengineering and informatics symposium, TBIS 2020

[8] Wei Q, Xiao X, Hou D et al (2008) Characterization of nonwoven material functionalized by sputter coating of copper. Surf Coat Technol 202:2535–2539. https://doi.org/10.1016/j.surfcoat.2007.09.022

[9] Periyasamy AP, Muthusamy LP, Militký J (2022) Neural network model applied to electromagnetic shielding effectiveness of ultra-light Ni/Cu coated polyester fibrous materials. Sci Rep 12:8609. https://doi.org/10.1038/s41598-022-12593-8

[10] Tom Cassauwers (2019) Is 5G bad for your health? It's complicated, say researchers. https://ec.europa.eu/research-and-innovation/en/horizon-magazine/5g-bad-your-health-its-complicated-say-researchers. Accessed 24 Sep 2022

[11] Lu G, Li X, Jiang H (1996) Electrical and shielding properties of ABS resin filled with nickel-coated carbon fibers. Compos Sci Technol 56:193–200. https://doi.org/10.1016/0266-3538(95)00143-3

[12] Tao L, Lee J, Akinwande D (2011) Nanofabrication down to 10 nm on a plastic substrate. J Vac Sci Technol B Nanotechnol Microelectron Mater Process Meas Phenom 29:06FG07. https://doi.org/10.1116/1.3662081

[13] Izydorczyk G, Mikula K, Skrzypczak D et al (2021) Potential environmental pollution from copper metallurgy and methods of management. Environ Res 197:111050. https://doi.org/10.1016/j.envres.2021.111050

[14] Dong BH, Hinestroza JP (2009) Metal nanoparticles on natural cellulose fibers: electrostatic assembly and in situ synthesis. ACS Appl Mater Interfaces 1:797–803. https://doi.org/10.1021/am800225j

[15] Emam HE, Ahmed HB, Bechtold T (2017) In-situ deposition of Cu 2 O micro-needles for biologically active textiles and their release properties. Carbohydr Polym 165:255–265. https://doi.org/10.1016/j.carbpol.2017.02.044

[16] Root W, Aguiló-Aguayo N, Pham T, Bechtold T (2018) Conductive layers through electroless deposition of copper on woven cellulose lyocell fabrics. Surf Coat Technol 348:13–21. https://doi.org/10.1016/j.surfcoat.2018.05.033

[17] Dastjerdi R, Montazer M, Shahsavan S (2009) A new method to stabilize nanoparticles on textile surfaces. Colloids Surf A Physicochem Eng Asp 345:202–210. https://doi.org/10.1016/j.colsurfa.2009.05.007

[18] Cao XG, Zhang HY (2012) Fabrication and performance of silver coated copper powder. Electron Mater Lett 8:467–470. https://doi.org/10.1007/s13391-012-1110-6

[19] Periyasamy AP, Yang K, Xiong X, et al (2019) Influence of EMI shielding on silane-coated conductive fabric. In: Textile bioengineering and informatics symposium proceedings 2019 - 12th textile bioengineering and informatics symposium, TBIS 2019. pp 67–71

[20] Periyasamy AP, Yang K, Xiong X et al (2019) Effect of silanization on copper coated milife fabric with improved EMI shielding effectiveness. Mater Chem Phys 239:122008. https://doi.org/10.1016/j.matchemphys.2019.122008

[21] Periyasamy AP, Vikova M, Vik M (2020) Spectral and physical properties organo-silica coated photochromic polyethylene terephthalate (PET) fabrics. J Text Inst 111:808–820. https://doi.org/10.1080/00405000.2019.1663633

[22] Periyasamy AP, Venkataraman M, Kremenakova D et al (2020) Progress in sol–gel technology for the coatings of

fabrics. Materials 13:1838. https://doi.org/10.3390/ma13081838

[23] ASTM D 4935–18: Standard test method for measuring the electromagnetic effectiveness of planar materials. https://www.astm.org/d4935-18.html

[24] Hu S, Wang D, Periyasamy AP et al (2021) Ultrathin multilayer textile structure with enhanced EMI shielding and air-permeable properties. Polymers (Basel) 13:4176. https://doi.org/10.3390/polym13234176

[25] Guglielmi M, Zenezini S (1990) The thickness of sol–gel silica coating obtained by dipping. J Non Cryst Solids 121:303–309. https://doi.org/10.1016/0022-3093(90)90148-F

[26] Lisa K, Mario A, Andrei J (2018) Handbook of sol–gel science and technology: processing, characterization, and applications. Springer International Publishing AG, Berlin, Germany. https://doi.org/10.1007/978-3-319-32101-1

[27] Gallo TA, Klein L (1986) Apparent viscosity of sol–gel processed silica. J Non Cryst Solids 82:198–204. https://doi.org/10.1016/0022-3093(86)90131-6

[28] Qian X, Song L, Bihe Y et al (2014) Organic/inorganic flame retardants containing phosphorus, nitrogen and silicon: preparation and their performance on the flame retardancy of epoxy resins as a novel intumescent flame retardant system. Mater Chem Phys 143:1243–1252. https://doi.org/10.1016/j.matchemphys.2013.11.029

[29] Tran TPT, Bénézet J-C, Bergeret A (2014) Rice and Einkorn wheat husks reinforced poly(lactic acid) (PLA) biocomposites: effects of alkaline and silane surface treatments of husks. Ind Crops Prod 58:111–124. https://doi.org/10.1016/j.indcrop.2014.04.012

[30] Vinisha Rani K, Sarma B, Sarma A (2017) Plasma sputtering process of copper on polyester/silk blended fabrics for preparation of multifunctional properties. Vacuum 146:206–215. https://doi.org/10.1016/j.vacuum.2017.09.036

[31] Xu W, Yuan X, Wei A et al (2018) Characterisation of PET nonwoven deposited with Ag/FC nanocomposite films. Surf Eng 34:838–845. https://doi.org/10.1080/02670844.2017.1382063

[32] Wei N, Cui H, Song Q et al (2016) Ag 2 O nanoparticle/TiO 2 nanobelt heterostructures with remarkable photo-response and photocatalytic properties under UV, visible and near-infrared irradiation. Appl Catal B 198:83–90. https://doi.org/10.1016/j.apcatb.2016.05.040

[33] Shao W, Li G, Zhu P et al (2018) Facile synthesis of low temperature sintering Ag nanopaticles for printed flexible electronics. J Mater Sci Mater Electron 29:4432–4440. https://doi.org/10.1007/s10854-017-8390-4

[34] Zheng J, Lin Z, Liu W et al (2014) One-pot synthesis of CuFe2O4 magnetic nanocrystal clusters for highly specific separation of histidine-rich proteins. J Mater Chem B 2:6207–6214. https://doi.org/10.1039/C4TB00986J

[35] (2010) D4935–10 ASTM standard test method for measuring the electromagnetic shielding effectiveness of planar materials. West Conshohocken, PA, USA

[36] DeMeo S (1997) Does copper metal react with acetic acid? J Chem Educ 74:844. https://doi.org/10.1021/ed074p844

[37] Okhrimenko DV, Budi A, Ceccato M et al (2017) Hydrolytic stability of 3-aminopropylsilane coupling agent on silica and silicate surfaces at elevated temperatures. ACS Appl Mater Interfaces 9:8344–8353. https://doi.org/10.1021/acsami.6b14343

[38] Arkles B, Pan Y, Larson GL, Singh M (2014) Enhanced hydrolytic stability of siliceous surfaces modified with pendant dipodal silanes. Chem Eur J 20:9442–9450. https://doi.org/10.1002/chem.201402757

[39] Noronha VT, Sousa FA, Souza Filho AG et al (2017) Influence of surface silanization on the physicochemical stability of silver nanocoatings: a large length scale assessment. J Phys Chem C 121:11300–11311. https://doi.org/10.1021/acs.jpcc.7b00706

[40] Sheng J, Zhang M, Xu Y et al (2016) tailoring water-resistant and breathable performance of polyacrylonitrile nanofibrous membranes modified by polydimethylsiloxane. ACS Appl Mater Interfaces 8:27218–27226. https://doi.org/10.1021/acsami.6b09392